

New constraints on time-dependent variations of fundamental constants using *Planck* data

Luke Hart^{1*} and Jens Chluba^{1†}

¹*Jodrell Bank Centre for Astrophysics, Alan Turing Building, University of Manchester, Manchester M13 9PL*

Accepted 2017 –. Received 2017 May 10.

ABSTRACT

Observations of the cosmic microwave background (CMB) today allow us to answer detailed questions about the properties of our Universe, targeting both *standard* and *non-standard* physics. In this paper, we study the effects of varying fundamental constants (i.e., the fine-structure constant, α_{EM} , and electron rest mass, m_e) around last scattering using the recombination codes CosmoRec and Recfast++. We approach the problem in a pedagogical manner, illustrating the importance of various effects on the free electron fraction, Thomson visibility function and CMB power spectra, highlighting various degeneracies. We demonstrate that the simpler Recfast++ treatment (based on a three-level atom approach) can be used to accurately represent the full computation of CosmoRec. We also include *explicit* time-dependent variations using a phenomenological power-law description. We reproduce previous *Planck* 2013 results in our analysis. Assuming constant variations relative to the standard values, we find the improved constraints $\alpha_{\text{EM}}/\alpha_{\text{EM},0} = 0.9993 \pm 0.0025$ (CMB only) and $m_e/m_{e,0} = 1.0039 \pm 0.0074$ (including BAO) using *Planck* 2015 data. For a redshift-dependent variation, $\alpha_{\text{EM}}(z) = \alpha_{\text{EM}}(z_0) [(1+z)/1100]^p$ with $\alpha_{\text{EM}}(z_0) \equiv \alpha_{\text{EM},0}$ at $z_0 = 1100$, we obtain $p = 0.0008 \pm 0.0025$. Allowing simultaneous variations of $\alpha_{\text{EM}}(z_0)$ and p yields $\alpha_{\text{EM}}(z_0)/\alpha_{\text{EM},0} = 0.9998 \pm 0.0036$ and $p = 0.0006 \pm 0.0036$. We also discuss combined limits on α_{EM} and m_e . Our analysis shows that existing data is not only sensitive to the value of the fundamental constants around recombination but also its first time derivative. This suggests that a wider class of varying fundamental constant models can be probed using the CMB.

Key words: recombination – fundamental physics – cosmology – CMB anisotropies

1 INTRODUCTION

Nowadays, measurements of the cosmic microwave background (CMB) anisotropies allow us to constrain the standard cosmological parameters with unprecedented precision (Bennett et al. 2013; Planck Collaboration et al. 2015a). This has opened a route for testing possible extensions to the Λ CDM model, e.g., related to the effective number of neutrino species and their mass (see Gratton et al. 2008; Battye & Moss 2014; Abazajian et al. 2015) and Big Bang Nucleosynthesis (Coc et al. 2013; André et al. 2014; Abazajian et al. 2016). In the analysis, we are furthermore sensitive to percent level effects in the recombination dynamics (Rubiño-Martín et al. 2010a; Shaw & Chluba 2011), which can be captured using advanced recombination codes such as CosmoRec and HyRec (Chluba & Thomas 2011; Ali-Haïmoud & Hirata 2011), again emphasizing the impressive precision of available cosmological datasets.

Our interpretation of the CMB measurements relies on several assumptions. The validity of general relativity and atomic physics around recombination are two evident ones. This encompasses a significant extrapolation of local physics, tested in the lab, to cos-

mological scales (both in distance and time). Albeit the successes of the Λ CDM cosmology, we know that simple extrapolation is currently not enough to explain the existence of dark matter and dark energy in our Universe. Similarly, it is important to test the validity of local physical laws in different regimes.

One of these tests is related to the *constancy of fundamental constants* (see Uzan 2003, 2011, for review). This could provide a glimpse at physics beyond the standard model, possibly shedding light on the presences of additional scalar fields and their coupling to the standard sector. Variations of the fine-structure constant, α_{EM} , and electron rest mass, m_e can directly impact CMB observables, as studied previously (e.g., Kaplinghat et al. 1999; Avelino et al. 2000; Battye et al. 2001; Avelino et al. 2001; Rocha et al. 2004; Martins et al. 2004; Scóccola et al. 2009; Menegoni et al. 2012) using modified versions of recfast (Seager et al. 1999). Similarly, changes of the gravitational constant can be considered (e.g., Lorén-Aguilar et al. 2003; Martins et al. 2010; Galli et al. 2011). Using *Planck* 2013 data, the values of α_{EM} and m_e around recombination were proven to coincide with those obtained in the lab to within $\approx 0.4\%$ for α_{EM} and $\approx 1 - 6\%$ for m_e (Planck Collaboration et al. 2015b). This is $\approx 2 - 3$ orders of magnitude weaker than constraints obtained from ‘local’ measurements (Bize et al. 2003; Rosenband et al. 2008; Bonifacio et al. 2014; Kotuš et al. 2017);

* Email: luke.hart@postgrad.manchester.ac.uk

† Email: jens.chluba@manchester.ac.uk

however, the CMB places limits during very different phases in the history of the Universe, some 380,000 years after the Big Bang, which complement these low-redshift measurements.

In this paper, we describe the effects of varying fundamental constants on the cosmological recombination history, focusing on variations of α_{EM} and m_e . These directly affect the atomic physics and radiative transfer in the recombination era ($z \approx 10^3$) and thus can be probed using CMB anisotropy measurements. We approach the problem in a pedagogical manner, illustrating the individual effects on the recombination dynamics in Sect. 2.1. We show that the full recombination calculation of CosmoRec can be accurately represented using a simple three-level atom approach, by introducing appropriate corrections functions (see Sect. 2.1.1). We discuss constant changes of α_{EM} and m_e , but also introduce a phenomenological power-law redshift-dependence of these parameters around recombination. The associated effects on the ionization history are distinct and thus can be individually constrained using CMB data.

The changes to the recombination codes are then propagated to the Thomson visibility function and the calculations of the CMB power spectra. Here we do not focus on the individual contributions to the CMB power spectrum deviations as these have been covered in previous literature (see Planck Collaboration et al. 2015b, Appendix B). However, we illustrate the overall effects and also highlight existing degeneracies between changes caused by α_{EM} , m_e and the average CMB temperature, T_0 . In Sect. 4, we present our constraints for different cases using *Planck* 2015 data. In particular, we find the CMB data to be sensitive not only to the value of the fundamental constants around recombination but also its first time derivative. We conclude in Sect. 5.

2 EFFECTS OF VARYING FUNDAMENTAL CONSTANTS ON IONIZATION HISTORY

In this section, we describe the effects of varying α_{EM} and m_e on the ionization history. We use modified versions of CosmoRec and Recfast++ (Chluba et al. 2010) for our computations¹, highlighting the importance of different effects and their individual impact on the free electron fraction, X_e .

2.1 How do α_{EM} and m_e enter the recombination problem?

Varying α_{EM} and m_e inevitably creates changes in the ionization history. Most importantly, the energy levels of hydrogen and helium depend on these constants, $E_i \propto \alpha_{\text{EM}}^2 m_e$, which directly affects the recombination redshift. In addition, atomic transition rates and photoionization/recombination rates are altered. Lastly, the interactions of photons and electrons through Compton and resonance scattering modify the radiative transfer physics. In an effective three-level atom approach (Zeldovich et al. 1968; Peebles 1968; Seager et al. 2000), the individual dependencies can be summarized as (e.g., Kaplinghat et al. 1999; Scóccola et al. 2009; Planck Collaboration et al. 2015b; Chluba & Ali-Haïmoud 2016)

$$\begin{aligned} \sigma_{\text{T}} &\propto \alpha_{\text{EM}}^2 m_e^{-2} & A_{2\gamma} &\propto \alpha_{\text{EM}}^8 m_e & P_{\text{S}} A_{1\gamma} &\propto \alpha_{\text{EM}}^6 m_e^3 \\ \alpha_{\text{rec}} &\propto \alpha_{\text{EM}}^2 m_e^{-2} & \beta_{\text{phot}} &\propto \alpha_{\text{EM}}^5 m_e & T_{\text{eff}} &\propto \alpha_{\text{EM}}^{-2} m_e^{-1}. \end{aligned} \quad (1)$$

Here, σ_{T} denotes the Thomson scattering cross section; $A_{2\gamma}$ is the two-photon decay rate of the second shell; α_{rec} and β_{phot} are the effective recombination and photoionization rates, respectively; T_{eff} is the effective temperature at which α_{rec} and β_{phot} need to be evaluated (see explanation below); $P_{\text{S}} A_{1\gamma}$ denotes the effective dipole

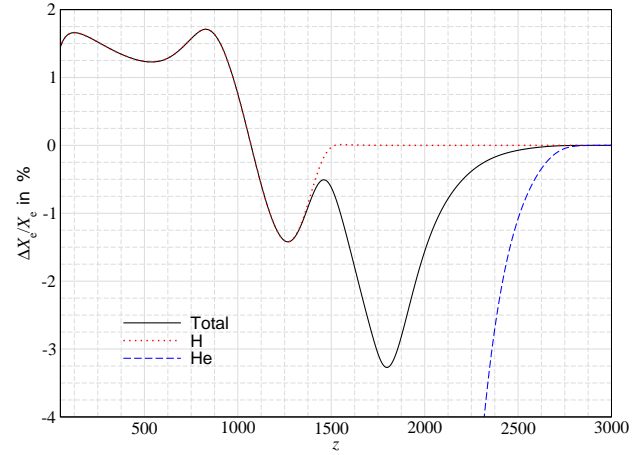


Figure 1. Relative difference in the free electron fractions of CosmoRec and Recfast++ (Recfast++ is used as reference) for the standard cosmology. The lines show the results for $X_e = X_e^{\text{H}} + X_e^{\text{He}}$ (black/solid), X_e^{H} (dotted/red) and X_e^{He} (dashed/blue).

transition rate for the main resonances (e.g., Lyman- α), which is reduced by the Sobolev escape probability, $P_{\text{S}} \leq 1$ (Sobolev 1960; Seager et al. 2000) with respect to the vacuum rate, $A_{1\gamma}$. For a more detailed account of how the transition rates depend on the fundamental constants we refer to Chluba & Ali-Haïmoud (2016) and the manual of HyRec (Ali-Haïmoud & Hirata 2011).

The scalings of σ_{T} , $A_{2\gamma}$ and $P_{\text{S}} A_{1\gamma}$ directly follow from their explicit dependencies on α_{EM} and m_e . The shown scalings of α_{rec} and β_{phot} reflect renormalisations of the transition rates, again stemming from their explicit dependencies on α_{EM} and m_e (e.g., Karzas & Latter 1961). However, these rates also depend directly on the ratio of the electron/photon temperature to the ionization threshold. This leads to an additional dependence on α_{EM} and m_e , which can be captured by evaluating these rates at rescaled temperature, with scaling indicated through T_{eff} . Overall, this leads to the effective dependence $\alpha_{\text{rec}} \propto \alpha_{\text{EM}}^{3.44} m_e^{-1.28}$ around hydrogen recombination (Chluba & Ali-Haïmoud 2016). The required photoionization rate, β_{phot} , is obtained using the detailed balance relation. Slightly different overall scalings for α_{rec} and β_{phot} were used in Planck Collaboration et al. (2015b), but we find the associated effect on the recombination history to be sub-dominant and limited to $z \lesssim 800$.

We also highlight that all atomic species are treated using hydrogenic scalings. For neutral helium, non-hydrogenic effects (e.g., fine-structure transitions, singlet-triplet couplings) become relevant (Drake 2006). However, the corrections should be sub-dominant and are neglected here.

We will illustrate the importance of the different terms in Eq. (1) in Sect. 2.2. This will show that in particular the changes in the energy scale, which are captured by rescaling the temperature, are crucial. We now continue by explaining the required modifications to Recfast++ and CosmoRec.

2.1.1 Modifications to Recfast++

Recfast++ is based on a simple three-level atom approach, similar to that of recfast (Seager et al. 1999). It evaluates three ordinary differential equations, evolving the free electron fraction contributions from hydrogen and singly-ionized helium, X_e^{H} and X_e^{He} , respectively, as well as the matter/electron temperature, T_e . Doubly-ionized helium is modeled using the Saha-relations.

¹ These codes are available at www.Chluba.de/CosmoRec.

As an added feature of the Recfast++ code, one can modify the obtained ionization history with a *correction function* to represent the full recombination calculation of CosmoRec (Rubiño-Martín et al. 2010b; Shaw & Chluba 2011). The required correction function between Recfast++ and CosmoRec is obtained as

$$X_e^C(z) \approx \left(1 + \frac{\Delta X_e(z)}{X_e^R(z)}\right) X_e^R(z) = f_{tot}(z) X_e^R(z), \quad (2)$$

where 'C' refers to CosmoRec, 'R' to Recfast++. In the code, the relative difference, $\Delta X_e/X_e^R = (X_e^C - X_e^R)/X_e^R$, is stored for the standard cosmology and then interpolated to obtain $f_{tot}(z)$. The relative difference, $\Delta X_e/X_e^R$, is illustrated in Fig. 1. For the standard cosmology, Recfast++ naturally allows a quasi-exact representation of the full calculation. For small variations around the standard cosmology, the correction-to-correction can be neglected so that this approach remains accurate in CMB analysis (Shaw & Chluba 2011; Planck Collaboration et al. 2015a).

All the modifications listed in Eq. (1) are readily incorporated to the simple Recfast++ equations. However, we found that for our purpose it was beneficial to treat the correction functions for hydrogen and helium separately, since in the transition regime between hydrogen and helium recombination ($z \approx 1600$) the free electron fraction departs from unity, which is physically not expected. This generalizes Eq. (2) to

$$X_e^C(z) \approx f_H(z) X_e^{H,R}(z) + f_{He}(z) X_e^{He,R}(z), \quad (3)$$

where we multiply each correction function term with its respective contribution to the total $X_e = X_e^H + X_e^{He}$. The individual correction functions are again obtained using relative differences with respect to the standard cosmology, $f_i(z) = 1 + \Delta X_e^i/X_e^{i,R}$. This is illustrated in Figure 1. At $z \approx 2500$, the helium correction sharply drops to $\Delta X_e^{He}/X_e^{He,R} \approx -100\%$ (i.e. $f_{He} \rightarrow 0$), indicating that helium rapidly recombines. This is related to hydrogen continuum absorption of helium photons, which is not taken into account in the standard treatment (Kholupenko et al. 2007; Switzer & Hirata 2008; Rubiño-Martín et al. 2008). Since hydrogen recombination occurs at lower redshifts, the hydrogen corrections tend to 0 at $z \gtrsim 1500$, while around $z \approx 1100$ radiative transfer corrections become visible (e.g., Fendt et al. 2009; Rubiño-Martín et al. 2010b, for overview).

At $z \lesssim 1500$, $f_{tot}(z) \approx f_H(z)$, while the features related to helium recombination corrections around $z \approx 1700$ are now represented directly by the helium correction function. Once added to Recfast++, it more fairly weights the helium corrections than the previous approach. In the code, one can chose between the two versions, but we find that when varying the fundamental constants, the new approach works best. It is furthermore important to interpret the correction functions as a function of temperature. This leads to the remapping $z \rightarrow z \times (\alpha_{EM}/\alpha_{EM,0})^{-2} (m_e/m_{e,0})^{-1}$, which captures the leading order transformation of radiative transfer corrections.

2.1.2 Modifications to CosmoRec

The modifications to Recfast++ were relatively straightforward. However, for CosmoRec this became a slightly bigger task. CosmoRec is built up as a modular system that allows each *module* to act as a plugin. In CosmoRec, the energies and transition rates within the hydrogen and neutral helium atoms needed to be rescaled with the previously mentioned scalings. These are represented by classes called `Atom` and `HeIAtom`, respectively, which include all the properties of given atomic levels, the collection of levels that form the atom and the ensemble of atoms around recombination. These can also be used as independent coding modules

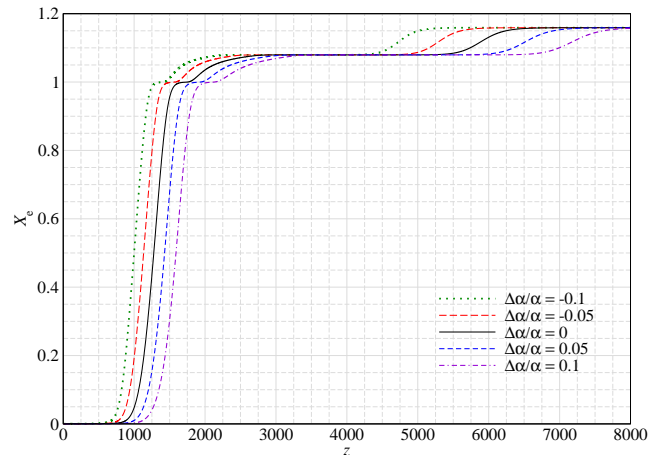


Figure 2. Ionization histories for different values of α_{EM} . The dominant effect is caused by modifications of the ionization threshold, which implies that for increased α_{EM} recombination finishes earlier. The curves were computed using Recfast++.

for atomic physics calculations. The neutral helium scalings with α_{EM} and m_e are modeled using hydrogenic expressions, which is expected to be accurate at the $\approx 0.1\% - 1\%$ level but omits higher order effects to the energy levels or transition rates.

After the atomic initializations, the effective transition rates (see Ali-Haïmoud & Hirata 2010, for details about the method) related to the multi-level atom need to be rescaled. In the code, these affect the effective recombination rates, $\mathcal{A}(T_\gamma, T_e)$, the photoionization rates, $\mathcal{B}(T_\gamma)$ and the inter-state transition rates, $\mathcal{R}(T_\gamma)$. Changes related to σ_T are again trivial to include.

During recombination, the processes occurring within the atoms are influenced by the temporal evolution of the background photon field. This complicates the recombination problem with the need for partial differential equations (PDEs) describing the radiative transfer (e.g. Chluba & Sunyaev 2007; Grachev & Dubrovich 2008; Chluba & Sunyaev 2009b; Hirata 2008; Hirata & Forbes 2009; Chluba & Sunyaev 2009a). When the fundamental constants are modified, one must again rescale the rates and energies required for the computations of the photon field. Similarly, the two-photon and Raman scattering profiles (Chluba & Sunyaev 2008; Hirata 2008; Chluba & Thomas 2011) have to be altered. We also carefully considered modifications to the neutral helium radiative transfer (Chluba et al. 2012). These effects can be separately activated in the latest version of CosmoRec (i.e. version 3.0 or higher).

2.2 Relevance of different effects for X_e

We now illustrate the importance of the individual effects in Eq. (1), for now assuming *constant* changes of α_{EM} and m_e . This will be generalized in Sect. 2.3. We shall start by focusing on changes caused by varying α_{EM} , parametrized as $\alpha_{EM} = \alpha_{EM,0}(1 + \Delta\alpha/\alpha)$. When all the terms relevant to the recombination problem are included, we obtain the ionization histories shown in Fig. 2 for different values of $\Delta\alpha/\alpha$. Increasing the fine structure constant shifts the moment of recombination toward higher redshifts. This agrees with the results found earlier in Kaplinghat et al. (1999), Battye et al. (2001) and Rocha et al. (2004) and can intuitively be understood in the following manner: $\Delta\alpha/\alpha > 0$ increases the transition energies between different atomic levels and the continuum. This increases

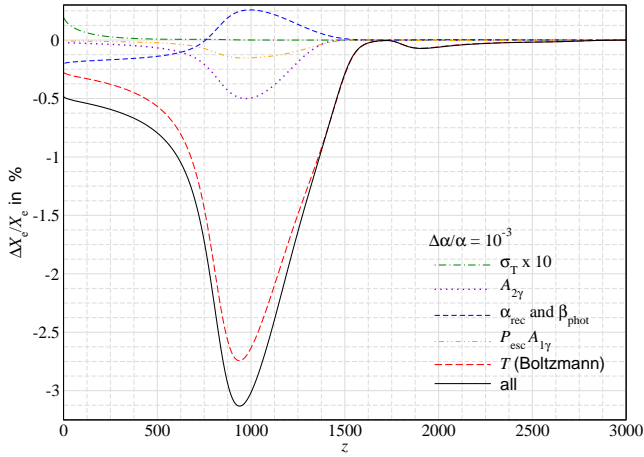


Figure 3. The relative changes in the ionization history for $\Delta\alpha/\alpha = 10^{-3}$ with respect to the standard case caused by different effects. `Recfast++` was used for the computations. The rescaling of temperature (\leftrightarrow mainly affecting the Boltzmann factors) yields $\Delta X_e/X_e \simeq -2.7\%$, dominating the total contributions, which peaks with $\simeq -3.1\%$ at $z \simeq 1000$. Note that the modification due to σ_T has been scaled by 10 to make it visible.

the energy threshold at which recombination occurs, hence increasing the recombination redshift, an effect that is basically captured by an effective temperature rescaling in the evaluation of the photoionization and recombination rates (see below).

The relative changes to the ionization history, $\Delta X_e/X_e$, for the different terms discussed in Section 2.1 are illustrated in Fig. 3. We chose a value for $\Delta\alpha/\alpha = 10^{-3}$, which leads to a percent-level effect on X_e . As expected, the biggest effect appears after rescaling the temperature for the evaluation of the photonization and recombination rates. More explicitly, this can be understood when considering the net recombination rate to the second shell, which can be written as $\Delta R_{\text{con}} = N_e N_p \alpha_{\text{rec}} - N_2 \beta_{\text{phot}} = \alpha_{\text{rec}} [N_e N_p - g(T_\gamma) N_2]$ (in full equilibrium, $\Delta R_{\text{con}} = 0$), where $g(T_\gamma) \propto T_\gamma^{3/2} e^{-h\nu_{2c}/kT_\gamma}$ with continuum threshold energy, $E_{2c} = h\nu_{2c}$. Here, the exponential factor (\leftrightarrow Boltzmann factor) is most important, leading to an enhanced effect once the replacement $T'_\gamma(z) = T_\gamma(z) \times (\alpha_{\text{EM}}/\alpha_{\text{EM},0})^{-2} (m_e/m_{e,0})^{-1}$ is carried out. For $\Delta\alpha/\alpha = 10^{-3}$, this gives $\Delta X_e/X_e \simeq -2.7\%$ at $z \simeq 1000$, which accounts for nearly all of the effect (cf., Fig. 3).

The second largest individual effect is due to the rescaling of the two-photon decay rate, $A_{2\gamma}$. This is expected since α_{EM} appears in a high power, $A_{2\gamma} \propto \alpha_{\text{EM}}^8$, and because the 2s-1s two-photon channel plays such a crucial role for the recombination dynamics (Zeldovich et al. 1968; Peebles 1968; Chluba & Sunyaev 2006b), allowing $\simeq 58\%$ of all hydrogen atoms to become neutral through this route (Chluba & Sunyaev 2006a). For $\Delta\alpha/\alpha = 10^{-3}$, we find $\Delta X_e/X_e \simeq -0.5\%$ at $z \simeq 1000$.

The normalizations of the recombination and photoionization rates (blue/dashed line) give rise to a net delay of $\Delta X_e/X_e \simeq 0.3\%$ at $z \simeq 1000$, which partially cancels the correction due to $A_{2\gamma}$. This is due to the stronger scaling of β_{phot} with α_{EM} than α_{rec} . At low redshifts ($z \lesssim 750$), recombination is again accelerated, indicating that a higher fraction of recombination events occurs, as the importance of photoionization ceases. The correction related to the Lyman- α channel is found to be $\simeq 3.3$ times smaller than for the two-photon channel, yielding $\Delta X_e/X_e \simeq -0.15\%$ at $z \simeq 1000$ (cf., Fig. 3).

Figure 3 also shows that the contributions from rescaling σ_T are very small and only become noticeable at low redshifts. At these

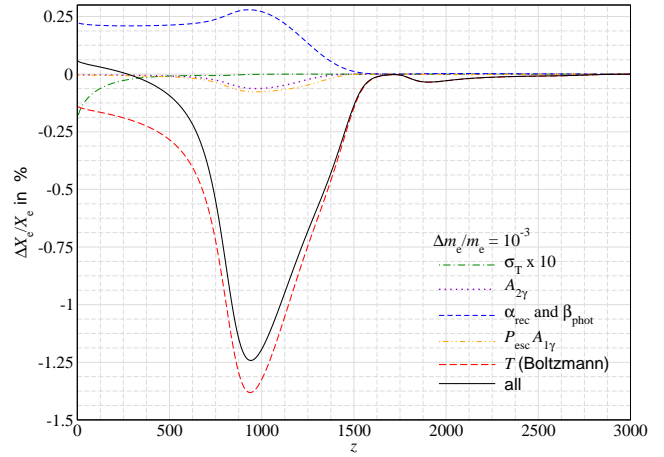


Figure 4. Same as in Fig. 3 but for $\Delta m_e/m_e = 10^{-3}$. The effective temperature rescaling again dominates the total change. Around $z \simeq 1000$, the total effect is $\simeq 2.5$ times smaller than for $\Delta\alpha/\alpha = 10^{-3}$.

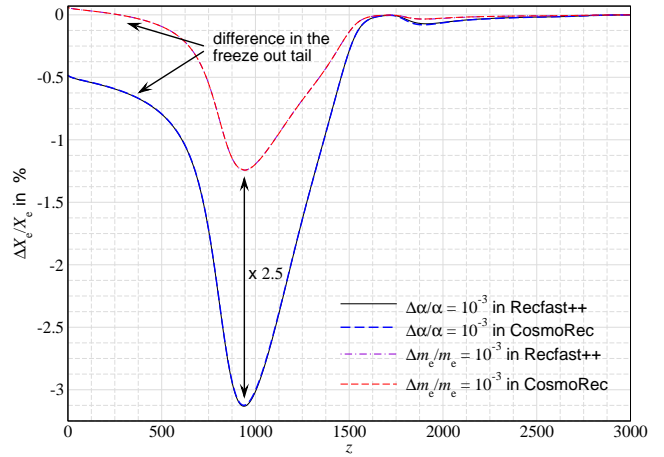


Figure 5. Comparison of the changes to the ionization history caused by variation of α_{EM} and m_e as computed with `Recfast++` and `CosmoRec`. Both codes agree extremely well (the lines practically overlap for the two cases), departing only at the level of $\simeq 0.1\%$ for X_e . For changes of m_e , the effect on the freeze-out tail is much smaller than for α_{EM} .

redshifts, the matter and radiation temperature begins to depart, giving $T_e < T_\gamma$. For larger α_{EM} , this departure is delayed, such that T_e stays longer close to T_γ . Hotter electrons recombine less efficiently, so that a slight delay of recombination appears (cf., Fig. 3). We find that this correction can in principle be neglected without affecting the results notably, but include it for completeness.

2.2.1 Changes due to variation of m_e

We now focus on changes caused by the effective electron mass, parametrized as $m_e = m_{e,0}(1 + \Delta m_e/m_e)$. Inspecting the scalings of Eq. (1), we expect the overall effect to be smaller than for α_{EM} . For example, the effect of temperature rescaling should be roughly half as large. Similarly, the effect due to rescaling $A_{2\gamma}$ should be roughly 8 times smaller, and so on. This is in good agreement with our findings (cf. Fig. 4). The net effect on X_e is about 2.5 times smaller than for α_{EM} around $z \simeq 1000$ (see Fig. 5 for a direct comparison). This suggests that the CMB constraint on m_e is weakened by a similar

factor. However, adding the rescaling of the Thomson cross section for the computation of the visibility function strongly enhances geometric degeneracies for m_e , such that the CMB only constraint on m_e is $\gtrsim 20$ times weaker than for α_{EM} (see Sect. 3.1.3).

A small difference related to the renormalizations of the photoionization and recombination rates (blue/dashed line) appears. For $\Delta m_e/m_e > 0$, the photoionization rate is increased and the recombination rate is reduced for these contributions [cf. Eq. (1)]. Both effects delay recombination (see Fig. 4). Thus, around $z \simeq 10^3$ the net effect is slightly larger than for α_{EM} . In contrast to α_{EM} , at late time no net acceleration of recombination occurs. These effects slightly modify the overall redshift dependence of the total X_e change, in addition lowering the effect in the freeze-out tail (see Fig. 5 for direct comparison). At the level $\Delta m_e/m_e \simeq 1\%$, additional higher order terms become important, allowing one to break the degeneracy between α_{EM} and m_e in joint analyses (see also Planck Collaboration et al. 2015b).

We note that we ignored the extra ρ_b/m_e scaling in the Compton cooling term for T_e , rescaling m_e in the atomic quantities only. When varying fundamental constants, dimensionless variables should furthermore be used (e.g., Rich 2015), so that an analysis of explicit m_e variations remains phenomenological.

2.2.2 Comparing Recfast++ and CosmoRec

We close by directly comparing the results for X_e obtained with Recfast++ and CosmoRec (Fig. 5). Both codes agree extremely well, departing by $\lesssim 0.1\%$ in X_e . Tiny differences in the resultant $\Delta X_e/X_e$ are visible around helium recombination ($z \simeq 1700$), which are related to radiative transfer effects that CosmoRec models explicitly. Similarly, around the maximum of the Thomson visibility function ($z \simeq 1100$), small percent-level differences in $\Delta X_e/X_e$ are present. These differences do not affect the computation of the CMB anisotropies at a significant level and thus our Recfast++ treatment is sufficient for the analysis presented in Sect. 4. We explicitly confirmed this by comparing the constraints obtained with the two recombination codes for α_{EM} and m_e , finding them to agree to high precision. Similarly, for the analysis of future CMB data (e.g. CMB Stage-IV), we deem our treatment with Recfast++ to suffice in these cases.

2.3 Adding an explicit redshift dependence to the variations

We extend our treatment of variation of fundamental constants by also considering an explicit redshift-dependence of α_{EM} and m_e , assuming a phenomenological power-law scaling around pivot redshift² $z_0 = 1100$. This could in principle be caused by the presence of a scalar field and its coupling to the standard particle sector during recombination. For α_{EM} , our model reads

$$\alpha_{\text{EM}}(z) = \alpha_{\text{EM}}(z_0) \left(\frac{1+z}{1100} \right)^p, \quad (4)$$

and similarly for m_e . For $p \ll 1$, we find a logarithmic dependence on redshift, $\alpha_{\text{EM}}(z) \approx \alpha_{\text{EM}}(z_0) (1 + p \ln[(1+z)/1100])$. Note that the rescaled value at the pivot redshift is not necessarily $\alpha_{\text{EM}}(z_0) \equiv \alpha_{\text{EM},0} \simeq 1/137$, but can also be varied. Here, p is a variable index that determines how the ionization history is stretched or compressed around the central redshift. We added this new option to Recfast++. Some examples are shown in Fig. 6. For $p > 0$, recombination is accelerated at $z \gtrsim 1000$ with respect to the standard

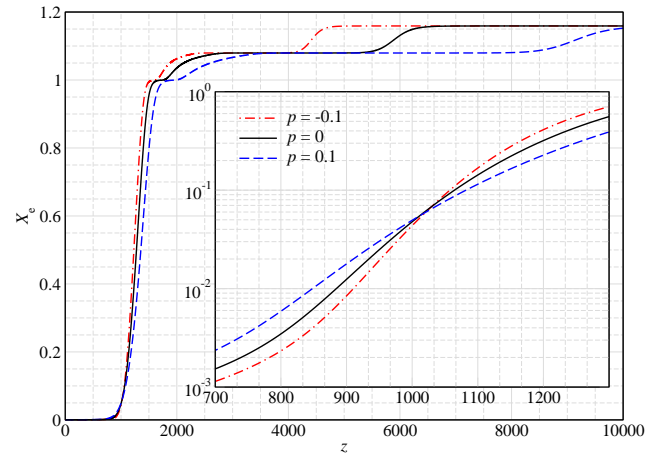


Figure 6. Ionization histories for redshift-dependent variation of the fine-structure constant, $\alpha_{\text{EM}}(z) = \alpha_{\text{EM}}(z_0) [(1+z)/1100]^p$. Here, we set $\alpha_{\text{EM}}(z_0)$ to the standard value, $\alpha_{\text{EM}}(z_0) \approx 1/137$, and only varied p . The different phases in the ionization history are stretched/compressed with respect to the standard case, depending on the chosen value for $p \neq 0$.

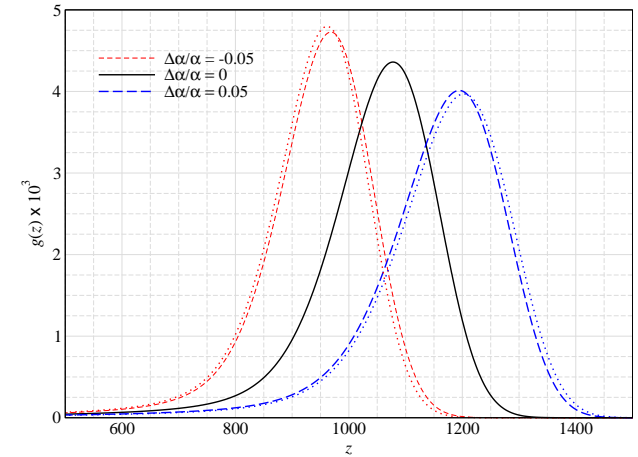


Figure 7. Visibility functions for a variety of fine structure constant values. A higher value of the fine structure constant leads to a broader visibility function, which simultaneously reduces its height. For illustration, the dotted lines exclude the rescaling of σ_T within CAMB.

case, while it is delayed at $z \lesssim 1000$. For $p \neq 0$, due to cumulative effects the change in X_e does not vanish at the pivot redshift. Also, the modification is very different to that of a constant shift of α_{EM} , predominantly affecting the width of the Thomson visibility function as opposed to the position (see Sect. 3). Thus, geometric degeneracies are found to be less important when constraining the value of p using CMB data (Sect. 4).

3 PROPAGATING THE EFFECTS TO THE CMB ANISOTROPIES

The temperature and polarization power spectra of the CMB depend on the dynamics of recombination through the ionization history, which defines the Thomson visibility function and last scattering surface (e.g., Sunyaev & Zeldovich 1970; Peebles & Yu 1970; Hu & Sugiyama 1996). Therefore, when varying α_{EM} and m_e , this leads to changes in the CMB power spectra. In this section,

² This choice de-correlates redshift-dependent and constant changes.

we show the modifications of the Thomson visibility function for the effects discussed in Section 2. The modified CMB temperature power spectra are then computed using CAMB (Lewis et al. 2000) for the standard cosmology (Planck Collaboration et al. 2015a). We briefly explain the main effects on the power spectra due to varying fundamental constants. Excluding modifications in the recombination dynamics, the CMB anisotropies still directly depend on the Thomson scattering cross section. We show that the changes from rescaling σ_T explicitly within CAMB are much smaller than those caused by modifications to the recombination dynamics. Still, they need to be included when deriving CMB constraints on fundamental constants (see also Planck Collaboration et al. 2015b), in particular when studying variations of m_e (see Sect. 4). We also present the changes of the CMB temperature power spectrum for the redshift-dependent variations of α_{EM} and m_e from Section 2.3.

3.1 Changes due to constant shifts of α_{EM} and m_e

Using the result for the ionization history computed with the modified version of Recfast++, one can calculate the Thomson visibility function, $g(z)$, defined as,

$$g(z) = \frac{d\tau}{dz} \exp[-\tau(z)]. \quad (5)$$

Here, $d\tau/dz$ is the differential Thomson optical depth. The Thomson visibility function can be interpreted as an effective probability distribution for a photon being last-scattered around redshift z . It is normalized such that $\int g(z) dz = 1$. From the changes in X_e described above, we expect that for $\Delta\alpha/\alpha > 0$ the maximum of the visibility function shifts toward higher redshifts. In Fig. 7, the visibility function is shown for constant $\Delta\alpha/\alpha = \{-0.05, 0, 0.05\}$. Indeed, the visibility function maximum moves to $z^{\max} \approx 1200$ for $\Delta\alpha/\alpha = 0.05$. The relative width, $\Delta z^{\text{FWHM}}/z^{\max}$, of the visibility function is roughly conserved.

3.1.1 Effects on the CMB anisotropies due to variations of α_{EM}

We illustrate the modifications to the CMB power spectrum for constant changes of α_{EM} in Fig. 8. We focus on the CMB temperature power spectra, as the effects on the polarization power spectra are qualitatively similar. Two main effects are visible. Firstly, the peaks of the power spectrum are shifted to smaller scales (larger ℓ) when $\Delta\alpha/\alpha > 0$. This happens because earlier recombination moves the last scattering surface towards higher redshifts, which decreases the sound horizon and increases the angular diameter distance to recombination (Kaplinghat et al. 1999; Battye et al. 2001). Secondly, for $\Delta\alpha/\alpha > 0$, the peak amplitudes are enhanced. This is mainly because earlier recombination suppresses the effect of photon diffusion damping on the anisotropies (Kaplinghat et al. 1999; Battye et al. 2001). For small $\Delta\alpha/\alpha$, we also illustrate the relative change of the temperature power spectrum in Fig. 10. The effect on the peak positions is more noticeable than the small overall tilt caused by changes related to diffusion damping.

3.1.2 Separate effect related to σ_T

The Thomson scattering cross section, σ_T , enters the problem in two ways. Firstly, it directly affects the recombination dynamics and thermal coupling between photons and baryons, as explained above (Sect. 2.2). These changes are taken into account when computing the recombination history, but turn out to be minor (Fig. 3 and 4) and can in principle be neglected. Secondly, σ_T also directly appears in the definition of the Thomson visibility function, $g(z)$, which is computed inside CAMB and has to be modified separately

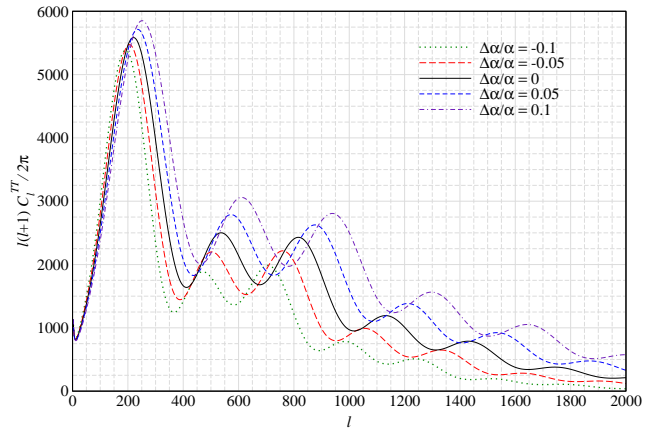


Figure 8. The CMB temperature power spectra for different values of α_{EM} . This shows that as the fine structure constant increases, the anisotropies shift toward smaller scales and higher amplitudes.

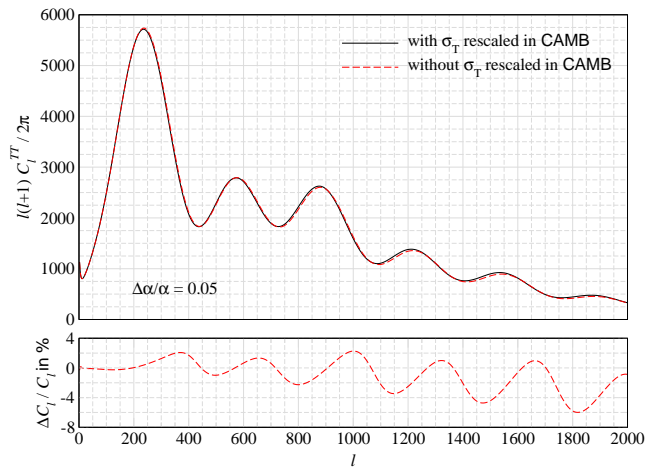


Figure 9. The CMB temperature power spectrum for $\Delta\alpha/\alpha = 0.05$ computed with and without explicit σ_T rescaling within CAMB. The upper panel shows the temperature power spectra and the lower illustrates the corresponding relative difference with respect to the full case.

(see Kaplinghat et al. 1999; Planck Collaboration et al. 2015b). The comparably small effect on $g(z)$ is illustrated in Fig. 7 for $\Delta\alpha/\alpha = \pm 0.05$, where the dotted lines exclude the rescaling of σ_T within CAMB. The corresponding changes to the TT power spectrum for $\Delta\alpha/\alpha = 0.05$ are shown in Fig. 9. In the considered ℓ range, the maximal relative difference is $|\Delta C_\ell/C_\ell| \approx 6\%$, which is more than one order of magnitude smaller than the effects due to direct changes in X_e discussed above. However, in particular when studying variations of m_e , this effect has to be included as otherwise the errors are strongly underestimated (see Sect. 4).

We included the effect of σ_T rescaling for the computation of the visibility in two independent ways. First, we consistently implemented these changes into CAMB by adding a rescaling function that targets the `akthom` components and Compton cooling terms within modules `f90` and `reionization.f90`. Second, we simply redefined the free electron fraction, X_e returned by the recombination code to CAMB as $X_e^* = (\alpha_{EM}/\alpha_{EM,0})^2 (m_e/m_{e,0})^{-2} X_e$. The two approaches gave extremely similar results for the power spectra and also final parameter constraints. The only real difference is that in the first approach, the corrections to the reionization history are in-

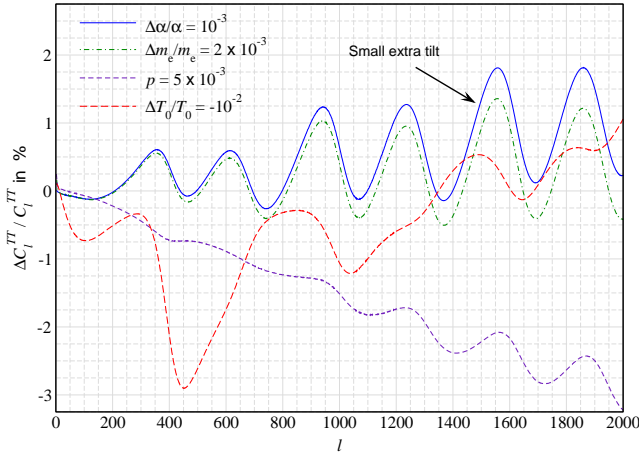


Figure 10. Comparison of the CMB TT power spectrum deviations when varying α_{EM} , m_e , T_0 and p . We chose $\Delta\alpha/\alpha = 10^{-3}$, $\Delta m_e/m_e = 2 \times 10^{-3}$, $\Delta T_0/T_0 = -10^{-2}$ and $p = 5 \times 10^{-3}$ (simultaneously for α_{EM} and m_e) to obtain effects at a similar level. Notice the small extra tilt when comparing the case for α_{EM} with m_e , which helps when constraining α_{EM} .

cluded more consistently, albeit not being modeled in a physical manner. For example, for $\Delta\alpha/\alpha > 0$, the reionization redshift reduces for fixed value of τ . In the second approach, the reionization history is not affected but the correction is minor. For our analysis, we used the explicit rescaling in CAMB including all terms.

3.1.3 Effects on the CMB anisotropies due to variations of m_e

We now briefly mention the changes caused by variation of m_e . As discussed above, for the free electron fraction the net changes are very similar to those for α_{EM} . Thus, one expects both changes in the visibility and CMB power spectra to be similar, albeit at a lower amplitude when $\Delta m_e/m_e \approx \Delta\alpha/\alpha \ll 1$. Indeed, we find the changes in the visibility function around its maximum to mimic those shown in Fig. 7 for variations of α_{EM} when setting $\Delta m_e/m_e \approx (2-3) \times \Delta\alpha/\alpha$. This is expected when comparing the main effect on X_e around redshift $z \approx 10^3$ for α_{EM} and m_e (Fig. 3 and Fig. 4), and suggests that the m_e -related changes in the CMB power spectra are also weakened by a similar factor. This is explicitly illustrated in Fig. 10, which shows that aside from a small overall tilt the changes in the CMB TT power spectra, $\Delta C_\ell/C_\ell(\Delta\alpha/\alpha)$ and $\Delta C_\ell/C_\ell(\Delta m_e/m_e)$, become almost indistinguishable when using $\Delta m_e/m_e \approx (2-3)\Delta\alpha/\alpha$. This presents a quasi-degeneracy between the two parameters and also suggests that naively the analysis for $\Delta\alpha/\alpha$ could be sufficient to estimate the errors for a corresponding analysis of m_e . However, when constraining m_e , enhanced geometric degeneracies (because of σ_T) push the error to the percent level. In this case, higher order terms become important and the degeneracy is again broken. When also adding information from BAO, the error on m_e is strongly reduced. In this regime, we indeed recover the simple scaling of the errors, $\sigma(\Delta m_e/m_e) \approx 3\sigma(\Delta\alpha/\alpha)$ [see Table 2].

3.1.4 Degeneracies between α_{EM} and T_0

Our previous discussion showed that a variation of α_{EM} and m_e directly affect the recombination redshift. The main effect can be captured by rescaling the Boltzmann factors using T_{eff} . This suggests that a change in the CMB monopole temperature, T_0 , could have a very similar effect. However, there is one crucial difference: T_0 also

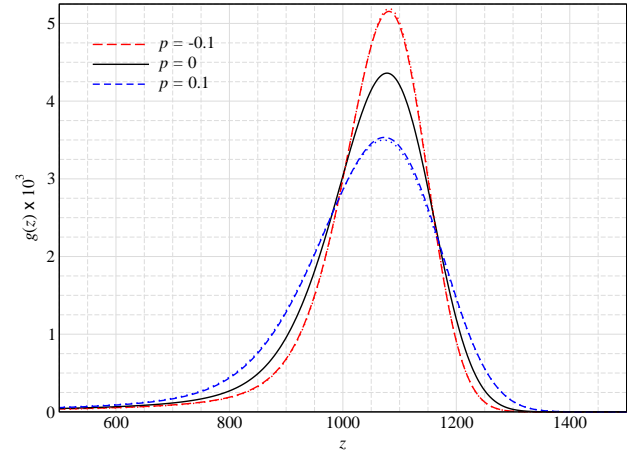


Figure 11. The visibility function $g(z)$ of the CMB for various cases of redshift dependent α_{EM} , parametrized as in Eq. (4). For $p < 0$, the recombination era is confined to a narrower redshift range as shown in Fig. 6, an effect that narrows the visibility function. Again, the dotted lines exclude the rescaling of σ_T within CAMB, which has a small overall impact here.

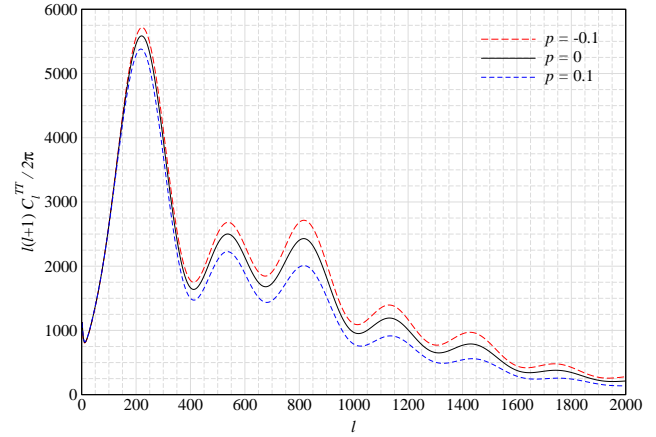


Figure 12. The CMB power spectrum for various values of the redshift power law index p for α_{EM} . Positive values of the p index lead to a suppression of the CMB peaks due to broadening of the recombination epoch.

affects the matter-radiation equality epoch. This modifies the integrated Sachs Wolfe (ISW) effect, which is most noticeable at low and intermediate ℓ and in principle should help one to break the degeneracy between changes of α_{EM} and T_0 . The relative change to the TT power spectrum is illustrated in Fig. 10, where we use $\Delta T_0/T_0 \approx -0.01$ to make the modifications comparable in amplitude. One can clearly see the enhanced effect at large angular scales due to the early and late ISW (see Fig. 3 in Challinor & Peiris 2009, for illustration of these contributions).

3.2 Changes due to redshift-dependent variations

We now consider redshift-dependent variations to α_{EM} and m_e , using the parametrization given by Eq. (4). We assume the standard values for α_{EM} and m_e at $z_0 = 1100$. In Fig. 11, we illustrate the effect on the Thomson visibility function for α_{EM} . Using $p < 0$, the visibility function narrows such that the effective width, $\Delta z^{\text{FWHM}}/z^{\text{max}}$, reduces. However, the changes in the position of the maximum value of $g(z)$ are negligible. This suggests that the

Parameter	<i>Planck</i> 2015	+ varying $\alpha_{\text{EM}}/\alpha_{\text{EM},0}$	+ varying p	+ varying $\alpha_{\text{EM}}/\alpha_{\text{EM},0}$ and p
$\Omega_{\text{b}}h^2$	0.02224 ± 0.00016	0.02225 ± 0.00016	0.02226 ± 0.00018	0.02223 ± 0.00019
$\Omega_{\text{c}}h^2$	0.1193 ± 0.0014	0.1191 ± 0.0018	0.1194 ± 0.0014	0.1193 ± 0.0020
$100\theta_{\text{MC}}$	1.0408 ± 0.0003	1.0398 ± 0.0035	1.0408 ± 0.0003	1.0406 ± 0.0051
τ	0.062 ± 0.014	0.063 ± 0.014	0.062 ± 0.014	0.063 ± 0.015
$\ln(10^{10}A_{\text{s}})$	3.057 ± 0.025	3.060 ± 0.027	3.058 ± 0.026	3.059 ± 0.027
n_{s}	0.9649 ± 0.0047	0.9668 ± 0.0081	0.9663 ± 0.0060	0.9666 ± 0.0081
$\alpha_{\text{EM}}/\alpha_{\text{EM},0}$	–	0.9993 ± 0.0025	–	0.9998 ± 0.0036
p	–	–	0.0008 ± 0.0025	0.0007 ± 0.0036
H_0 [km s ⁻¹ Mpc ⁻¹]	67.5 ± 0.6	67.2 ± 1.0	67.5 ± 0.6	67.3 ± 1.4

Table 1. Constraints on the standard Λ CDM parameters and the fundamental constant parameters $\alpha_{\text{EM}}/\alpha_{\text{EM},0}$ and p for different combinations of parameters. The standard *Planck* runs include the *TTTEEE* likelihood along with the low ℓ polarization and CMB lensing likelihoods and the errors are the 68% limits.

changes in the positions of the peaks in the CMB power spectra are minor, while the *blurring* related to the finite thickness of the last scattering surface is reduced³. The separate effect of rescaling σ_{T} inside CAMB is also illustrated in Fig. 11, an effect that we find to have a negligible impact when constraining the value of p alone. Similar comments apply for changes to m_{e} .

We show the changes in the CMB temperature power spectra due to redshift-dependent variations of α_{EM} in Fig. 12. When we choose $p < 0$, the CMB peaks are amplified. This is expected from the reduced width, $\Delta z^{\text{FWHM}}/z^{\text{max}}$, of the visibility function in Fig. 11. Similarly, for $p > 0$, a larger damping effect due to blurring is found. The relative change of C_{ℓ} for $p = 5 \times 10^{-3}$ is shown in Fig. 10. The smoothness of the titled curve indicates that blurring of anisotropies is indeed the dominant effect. Again, similar effects are found for changes to m_{e} .

4 CONSTRAINTS USING PLANCK DATA

We now constrain the variations of α_{EM} , m_{e} and p discussed in Sec. 3 using CosmoMC (Lewis & Bridle 2002) with the *Planck* 2015 data⁴. We sample over the acoustic angular scale, θ_{MC} . Although for this specific analysis, H_0 is expected to de-correlate quicker, we did not encounter any problems. We find that the constraints derived for α_{EM} and m_{e} are consistent with those for *Planck* 2013 data (Planck Collaboration et al. 2015b), albeit here with slightly improved errors. We also show the new constraints for our redshift dependent model of α_{EM} . Our marginalized constraints are summarized in Tables 1 and 2. For comparison, the standard Λ CDM parameter run for the *Planck* data is also given. For each run, we show the derived H_0 parameter. The 2D parameter contours are shown in Fig. 13.

4.1 Constraining α_{EM} and m_{e}

When varying α_{EM} , assuming constant $\Delta\alpha/\alpha$, along with the 6 standard cosmological parameters, we find the marginalized parameter values in the second column of Table 1. These show that $\alpha_{\text{EM}}/\alpha_{\text{EM},0}$ is equal to unity well within the 68% limit. The errors on θ_{MC} increases by about one order of magnitude, due to the added uncertainty in the distance to the last scattering surface. We also find a slight increase in the errors of the scalar spectral index, n_{s} , which interacts with the modifications to the photon diffusion damping

scale caused by α_{EM} . Similarly, the error of the cold dark matter density, $\Omega_{\text{c}}h^2$, increases slightly, due to geometric degeneracies. The other parameters (i.e., τ and A_{s}) are largely unaltered by the addition of α_{EM} as a parameter (see Fig. 13). This highlights the stability and consistency of the data with respect to non-standard extensions of the cosmological model.

Although the contributions from σ_{T} appear to have a negligible effect on the C_{ℓ} (see Fig. 9), we find that the inclusion of this effect improves the errors on α_{EM} by $\simeq 30\%$. The small effect on the power spectra hinders some of the degeneracy between θ_{MC} and $\alpha_{\text{EM}}/\alpha_{\text{EM},0}$, as pointed out in previous analyses (e.g. Planck Collaboration et al. 2015b). For example, the marginalized value of $\alpha_{\text{EM}}/\alpha_{\text{EM},0}$ changes from 0.9988 ± 0.0033 to 0.9993 ± 0.0025 when including σ_{T} rescaling within CAMB⁵. Future CMB missions have the potential to improve this constraint by another factor of $\simeq 4 - 5$ (Di Valentino et al. 2016).

For constant changes to m_{e} , we obtain the results given in the first two columns of Table 2. Using 2015 CMB data alone, we find $m_{\text{e}}/m_{\text{e},0} = 0.961^{+0.046}_{-0.072}$ and $H_0 = 60^{+8}_{-16}$ km s⁻¹ Mpc⁻¹, which is consistent with the corresponding result (*Planck*+WP+lensing), $m_{\text{e}}/m_{\text{e},0} = 0.969 \pm 0.055$ and $H_0 = (62 \pm 10)$ km s⁻¹ Mpc⁻¹, given in Planck Collaboration et al. (2015b). Following the *Planck* 2013 analysis, we used a flat prior $H_0 = [40, 100]$ km s⁻¹ Mpc⁻¹. We note that at the lower end of this range this leads to a slight truncation of the posterior distribution for H_0 . Also, our errors for the CMB-only analysis remain asymmetric, even when repeating the *Planck* 2013 run, for which we find $m_{\text{e}}/m_{\text{e},0} = 0.964^{+0.054}_{-0.068}$ and $H_0 = 61^{+9.5}_{-15}$ km s⁻¹ Mpc⁻¹. The remaining difference between the errors is not negligible and should be investigated further. We already confirmed that it is not related to the slightly different scalings for α_{rec} and β_{phot} used in Planck Collaboration et al. (2015b), but leave a more detailed study to future work.

For varying m_{e} , the values of H_0 and m_{e} are both biased low when only using CMB data (see also Planck Collaboration et al. 2015b). Interestingly, this bias is removed when neglecting the effect of σ_{T} on the Thomson visibility, for which we find $H_0 = (67.0 \pm 1.6)$ km s⁻¹ Mpc⁻¹ and $m_{\text{e}}/m_{\text{e},0} = 0.9970 \pm 0.0098$. This treatment also significantly decreases the errors due to reduced geometric degeneracies, which highlights the importance of σ_{T} for the computation of constraints on variations of m_{e} . At the level of $\Delta m_{\text{e}}/m_{\text{e}} \simeq 1\%$, also non-linear corrections become noticeable.

³ An explanation of this damping effect can be found in Mukhanov (2004).

⁴ When quoting *Planck* 2015 data we usually refer to the likelihood *Planck* 2015 *TTTEEE*+lowP+lensing. For *Planck* 2013, we imply *Planck*+WP+lensing as baseline.

⁵ The former result was also presented in the initial versions of Di Valentino et al. (2016), but now agrees with latter.

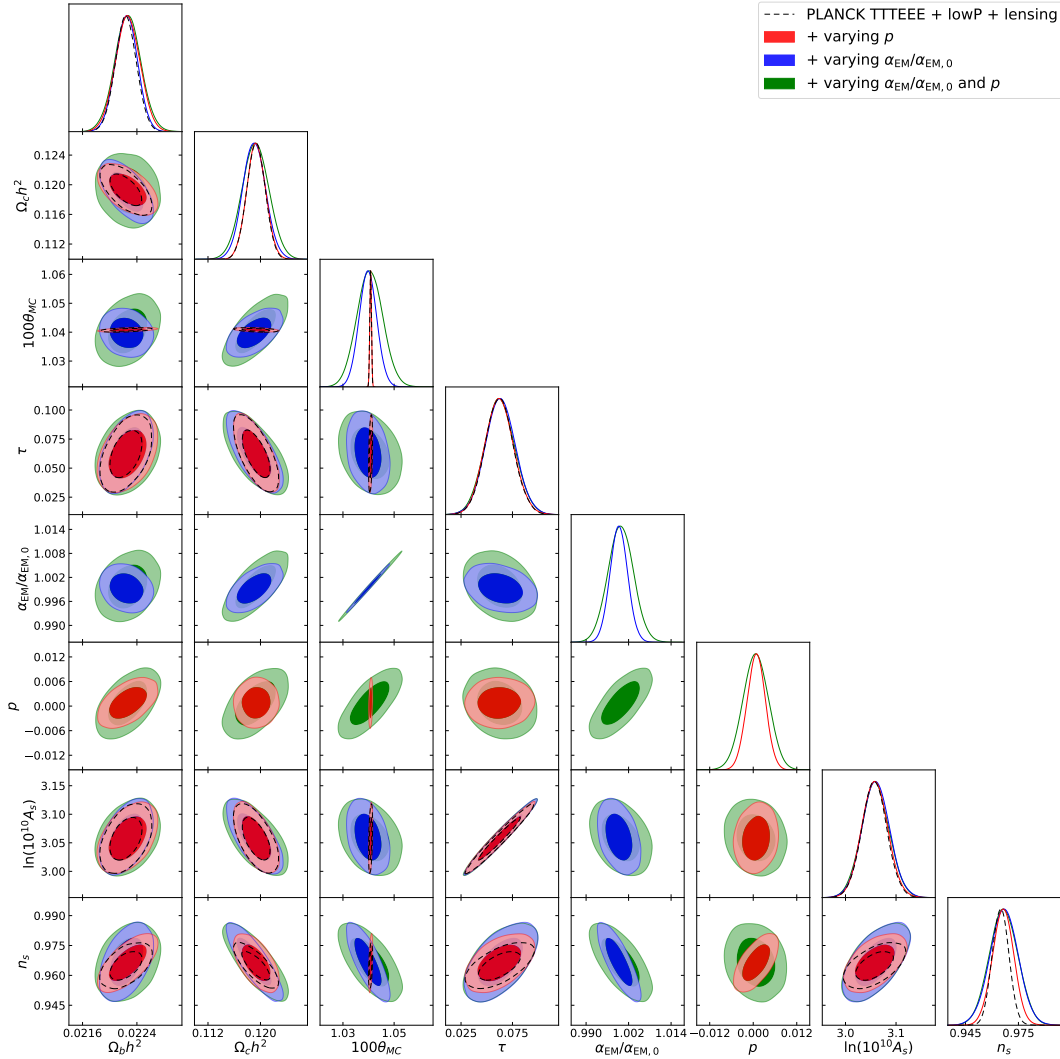


Figure 13. The full contours with the $TTTEEE$ + lowP + lensing likelihoods from *Planck* 2015. The standard Λ CDM run (black, dotted) is shown alongside the added variations in α_{EM} (blue), p (red) and the combination of the two parameters (green).

Parameter	<i>Planck</i> 2015 + $m_e/m_{e,0}$	<i>Planck</i> 2015 + BAO + $m_e/m_{e,0}$	<i>Planck</i> 2015 + $\alpha_{EM}/\alpha_{EM,0}$ and $m_e/m_{e,0}$	<i>Planck</i> 2015 + BAO + $\alpha_{EM}/\alpha_{EM,0}$ and $m_e/m_{e,0}$
$\Omega_b h^2$	$0.0213^{+0.0011}_{-0.0017}$	0.02233 ± 0.00018	$0.0214^{+0.00099}_{-0.0017}$	0.02238 ± 0.00020
$\Omega_c h^2$	$0.1146^{+0.0059}_{-0.0087}$	0.1202 ± 0.0022	$0.1144^{+0.0057}_{-0.0090}$	0.1200 ± 0.0023
θ_{MC}	$1.012^{+0.036}_{-0.051}$	1.0435 ± 0.0052	$1.011^{+0.034}_{-0.054}$	1.0431 ± 0.0053
τ	0.057 ± 0.015	0.080 ± 0.017	0.058 ± 0.015	0.082 ± 0.019
$\ln(10^{10} A_s)$	3.044 ± 0.029	3.095 ± 0.033	3.048 ± 0.031	3.100 ± 0.037
n_s	0.9639 ± 0.0048	0.9647 ± 0.0046	0.9663 ± 0.0078	0.9678 ± 0.0085
$\alpha_{EM}/\alpha_{EM,0}$	–	–	0.9990 ± 0.0025	0.9989 ± 0.0026
$m_e/m_{e,0}$	$0.961^{+0.046}_{-0.072}$	1.0039 ± 0.0074	$0.962^{+0.044}_{-0.074}$	1.0056 ± 0.0080
H_0 [km s $^{-1}$ Mpc $^{-1}$]	60^{+8}_{-16}	68.1 ± 1.3	60^{+7}_{-16}	68.1 ± 1.3

Table 2. Constraints on the standard Λ CDM parameters and the fundamental constant parameters $\alpha_{EM}/\alpha_{EM,0}$ and $m_e/m_{e,0}$ for different combinations of parameters. The standard *Planck* runs include the $TTTEEE$ likelihood along with the low ℓ polarization and CMB lensing likelihoods and the errors are the 68% limits. We also show the results when adding BAO data.

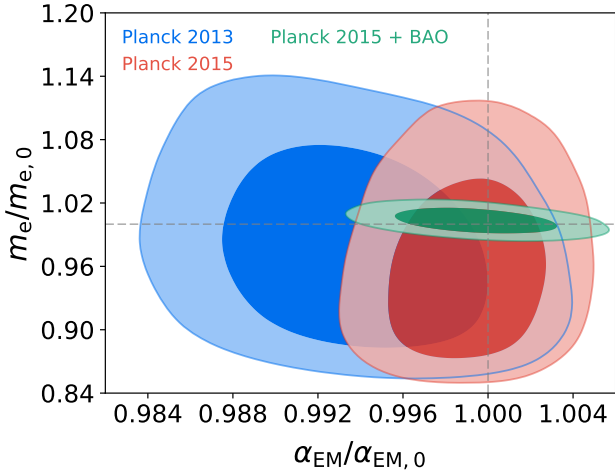


Figure 14. The joint likelihood contour for m_e and α_{EM} for *Planck* 2013+WP+lensing and *Planck* 2015 *TTTEEE*+lowP+lensing data. The *Planck* 2015 contours are narrowed in the α_{EM} direction due to improved polarization information over *Planck* 2013. Adding BAO data to *Planck* 2015 further improves the constraint in particular on m_e . The dashed lines indicate $\Delta m_e/m_e = \Delta \alpha/\alpha = 0$ for reference.

Given the large geometric degeneracy, we also ran the constraint for m_e when adding BAO data (see Table 2). In this case, we obtained⁶ $m_e/m_{e,0} = 1.0039 \pm 0.0074$, which, albeit improved error, is consistent with the result $m_e/m_{e,0} = 1.004 \pm 0.011$ given in Planck Collaboration et al. (2015b). The value of H_0 returns to the standard CMB value when adding BAO data. For this combination of datasets, we also find that the error on m_e is ≈ 3 times larger than the corresponding error on α_{EM} , as naively expected from the similarity of the changes in the *TT* power spectrum (Fig. 10).

4.1.1 Simultaneously constraining α_{EM} and m_e

We finish our analysis of this section by simultaneously varying α_{EM} and m_e (see Table 2 for our constraints). The responses in the CMB power spectra are quite similar for $\Delta\alpha/\alpha \approx \Delta m_e/m_e \approx 10^{-3}$ (see Fig. 10), suggesting a significant degeneracy between α_{EM} and m_e . However, combined CMB-only constraints are obtained when non-linear corrections in particular for m_e become noticeable, so that both parameters can be simultaneously constrained.

The strong degeneracies between α_{EM} and m_e are substantially reduced when going from *WMAP* to *Planck* 2013, as already described in Planck Collaboration et al. (2015b). In Fig. 14, we show our contours for *Planck* 2013 and 2015 data. The non-Gaussian shapes of the contours are reminiscent of the non-linear terms mentioned above. We find $\alpha_{EM}/\alpha_{EM,0} = 0.9990 \pm 0.0025$ and $m_e/m_{e,0} = 0.962^{+0.044}_{-0.074}$ for *Planck* 2015. This improves over our constraint for *Planck* 2013, $\alpha_{EM}/\alpha_{EM,0} = 0.9936 \pm 0.0042$ and $m_e/m_{e,0} = 0.977^{+0.056}_{-0.071}$, which is in good agreement with the result given in Planck Collaboration et al. (2015b) for this case. The improvement is mainly due to better polarization information.

As for the analysis of m_e , we can see that CMB data alone tends towards low values of H_0 and $m_e/m_{e,0}$. This bias is removed when adding BAO, for which we find $\alpha_{EM}/\alpha_{EM,0} = 0.9989 \pm 0.0026$, $m_e/m_{e,0} = 1.0056 \pm 0.0080$ and $H_0 = 68.1 \pm 1.3$. These numbers are consistent with the standard *Planck* 2015 cosmology (see Table 2).

⁶ Adding lensing did not affect the constraint at a very significant level.

4.2 Constraining the redshift dependence of α_{EM} and m_e

Next, we consider redshift-dependent variations of α_{EM} , using the parametrization in Eq. (4) with $\alpha_{EM}(z_0) = \alpha_{EM,0}$. The constraints for this case are shown in third column of Table 1. Since varying p mainly affects the tilt of the CMB power spectra, degeneracies with n_s and $\Omega_b h^2$ are expected. Indeed, we find the errors of these parameters to be slightly increased, while all other parameters are basically unaffected (see Fig. 13). In particular, the θ_{MC} contours still mimic the *Planck* 2015 contours without varying α_{EM} as shown by the red and dotted black line in Fig. 13. This already indicates that the individual effects of variations of $\alpha_{EM}(z_0)$ and p should be separable. When varying both parameters independently, we obtain the constraints indicated by the last column in Table 1. Albeit slightly weakened, we can independently constrain $\alpha_{EM}(z_0)$ and p .

Carrying out a similar analysis for m_e , setting $m_e(z_0) = m_{e,0}$ we find $p = 0.0006 \pm 0.0044$ for *Planck* 2015 *TTTEEE*+lowP+lensing data. This is roughly 2 times weaker than for α_{EM} , consistent with naive analysis of the free electron fraction scaling around $z \approx 1100$ (see Fig. 5). Also varying $m_e(z_0)$, we obtain $m_e/m_{e,0} = 0.960^{+0.046}_{-0.071}$ and $p = 0.0012^{+0.0047}_{-0.0042}$. When adding BAO data, this improves to $m_e/m_{e,0} = 1.0023 \pm 0.0074$ and $p = 0.0007 \pm 0.0043$, again with no significant biases in the standard parameters with respect to the *Planck* 2015 cosmology remaining.

5 CONCLUSIONS

Current observations provide us with very precise cosmological datasets, that allow us to ask detailed questions about the conditions of the Universe around the recombination epoch. In this paper, we analyzed the different effects on the recombination problem when varying α_{EM} and m_e . We explained the modifications to the recombination codes, *Recfast++* and *CosmoRec*, that are required to vary these constants in an easy and efficient way. In particular, we developed an improved correction function treatment for *Recfast++* (Sect. 2.1.1), which allows us to accurately represent the full computation of *CosmoRec* (cf. Fig. 5). We find that the remaining differences between the two recombination codes can in principle be neglected at the current level of precision.

For constant $|\Delta\alpha/\alpha| \lesssim 1\%$, we find a total effect on the ionization history of $\Delta X_e/X_e \approx -27 \times \Delta\alpha/\alpha$ at $z \approx 10^3$ (see Fig. 3). This is dominated by the required rescaling of the ionization potential in the equilibrium Boltzmann factors. Other corrections related to $A_{2\gamma}$, α_{rec} and β_{phot} contribute at the $\sim 10\%$ level to this net effect. We also find that when varying α_{EM} and m_e the associated direct changes to the recombination history caused by scaling the Thomson scattering cross section are negligible (see Fig. 3). We still include this correction in our analysis for consistency.

When varying m_e , we find the net effect on X_e around $z \approx 10^3$ to be comparable to that of varying α_{EM} for $\Delta m_e/m_e \approx 2.5 \times \Delta\alpha/\alpha$. The net change of X_e in the freeze-out tail is smaller than for α_{EM} (see Fig. 4 and 5), an effect that is related to the different scaling of α_{rec} and β_{phot} with α_{EM} and m_e (see Sect. 2.2).

We also include explicit redshift-dependent variations of α_{EM} . This has a very different effect on the ionization history around recombination. Instead of shifting the recombination redshift during hydrogen recombination, the ionization history is stretch/compressed differentially, depending on the chosen parameters (see Fig. 6). This has a distinct effect on the CMB anisotropies that can be separated from the one for constant variations.

The propagation of the modifications in the recombination

dynamics through to the Thomson visibility function and CMB anisotropies is also illustrated (see Sect. 3). For constant $\Delta\alpha/\alpha$, our results are in agreement with previous analyses (e.g., Kaplinghat et al. 1999; Battye et al. 2001). We find that the changes to the CMB temperature power spectrum caused by variation of α_{EM} and m_e are practically degenerate when $\Delta m_e/m_e \approx (2-3) \times \Delta\alpha/\alpha \approx 10^{-3}$ (see Fig. 10). However, combined constraints on α_{EM} and m_e are obtained in a regime in which higher order terms especially for m_e become relevant (Sect. 4.1.1), making them again distinguishable. Changes caused by directly varying the CMB monopole temperature, T_0 , should in principle be distinguishable due to the ISW effects (see Sect. 3.1.4 and Fig. 10), although we do not explore this possibility in more detail here.

We also illustrate the effect of redshift-dependent changes. Instead of shifting the maximum of the Thomson visibility function (cf. Fig. 7), a power-law variation of α_{EM} with redshift (see Eq. 4) causes a change in the width of the visibility function (see Fig. 11). This primarily modifies the blurring of CMB anisotropies (compare Fig. 8 and 12) and can thus be distinguished.

In Sect. 4, we present our constraints on different cases using *Planck* 2015 data. Our results (see Table 1 and 2) for constant $\Delta\alpha/\alpha$ and $\Delta m_e/m_e$ are consistent with those given in Planck Collaboration et al. (2015b). We obtain the updated individual constraints $\alpha_{\text{EM}}/\alpha_{\text{EM},0} = 0.9993 \pm 0.0025$ and $m_e/m_{e,0} = 0.961^{+0.046}_{-0.072}$ using *Planck* 2015 data alone. Also adding BAO data, we find $\alpha_{\text{EM}}/\alpha_{\text{EM},0} = 0.9997 \pm 0.0023$ and $m_e/m_{e,0} = 1.0039 \pm 0.0074$. When varying m_e , the addition of BAO data removes the bias in H_0 towards low values, making the results consistent with the standard *Planck* cosmology (Table 2). Simultaneous constraints when varying both α_{EM} and m_e are presented in Sect. 4.1.1.

Although we show that the effect of rescaling σ_{T} for the computation of the Thomson visibility function is quite small (cf., Fig. 7 and 11), this effect should be included in the analysis (see also Planck Collaboration et al. 2015b). For models with varying α_{EM} , we find that this effect improves the constraint by $\approx 30\%$. The change is more dramatic when varying m_e . Here, we find that neglecting the rescaling of σ_{T} leads to a significant underestimation of the error (a factor $\gtrsim 5$) unless BAO data is added. This is due to enhanced geometric degeneracies caused by the scaling of σ_{T} in the visibility function calculation (see Sect. 4.1).

Allowing for power-law redshift dependence of α_{EM} around $z_0 = 1100$ with $\alpha_{\text{EM}}(z_0) = \alpha_{\text{EM},0}$, we find the new constraint, $p = 0.0008 \pm 0.0025$, on the power-law index. When varying both $\alpha_{\text{EM}}(z_0)$ and p , we obtain $\alpha_{\text{EM}}(z_0)/\alpha_{\text{EM},0} = 0.9998 \pm 0.0036$ and $p = 0.0006 \pm 0.0036$ (see Table 1). Similarly, for m_e we find $p = 0.0006 \pm 0.0044$ (CMB only) assuming $m_e(z_0) = m_{e,0}$. Varying both $m_e(z_0)$ and p we obtain $m_e/m_{e,0} = 1.0023 \pm 0.0074$ and $p = 0.0007 \pm 0.0043$ when also adding BAO data (see Sect 4.2). All these results are fully consistent with the standard values, highlighting the impressive precision, stability and consistency of the data with respect to non-standard extensions. This also suggests that a wider class of varying fundamental constant models can in principle be probed using the CMB, possibly with more complex redshift-dependence (e.g., phase transition, spikes or higher order temporal curvature).

Modified recombination physics can also be investigated using CMB spectral distortions. For the future, we aim to continue this study with the cosmological recombination radiation (e.g., Rubiño-Martín et al. 2006; Chluba & Sunyaev 2006a; Sunyaev & Chluba 2009). Modeling these variations in CosmoSpec (Chluba & Ali-Haïmoud 2016) will enlighten us on how the fundamental constants change the recombination spectrum and provide us with another

dataset for constraints. This could allow us to alleviate existing parameter degeneracies and further deepen our understanding of the recombination epoch, allowing us to confront clear theoretical predictions with direct observational evidence. This might also open the possibility to probe the redshift-dependence of the fundamental constants at even earlier phases through the individual effects on hydrogen and helium recombination (e.g., see Fig. 6 for the effect on X_e), which would remain inaccessible otherwise. One could furthermore refine constraints on spatial variations of fundamental constants. We look forward to exploring these opportunities.

ACKNOWLEDGEMENTS

We cordially thank the referee for their comments on the paper and the suggestions to more carefully consider the effect of σ_{T} and extend our analysis for m_e . We also thank Marcos Ibañez from IAC for his discussion surrounding CosmoMC and how to optimise the sampling, given an increase in parameters. We extend thanks to Richard Battye, Carlos Martins and James Rich for discussion pertaining to previous studies of fundamental constant variations. We would also like to thank the Jodrell Bank Centre for Astrophysics, University of Manchester for the use of the FORNAX cluster as a tool to help reduce convergence runtimes. LH is funded by the Royal Society through grant RG140523. JC is supported by the Royal Society as a Royal Society University Research Fellow at the University of Manchester, UK.

REFERENCES

- Abazajian K. N. et al., 2016, ArXiv:1610.02743
 Abazajian K. N. et al., 2015, *Astroparticle Physics*, 63, 66
 Ali-Haïmoud Y., Hirata C. M., 2010, *Phys.Rev.D*, 82, 063521
 Ali-Haïmoud Y., Hirata C. M., 2011, *Phys.Rev.D*, 83, 043513
 André P. et al., 2014, *JCAP*, 2, 6
 Avelino P. P. et al., 2001, *Phys.Rev.D*, 64, 103505
 Avelino P. P., Martins C. J. A. P., Rocha G., Viana P., 2000, *Phys.Rev.D*, 62, 123508
 Battye R. A., Crittenden R., Weller J., 2001, *Phys.Rev.D*, 63, 043505
 Battye R. A., Moss A., 2014, *Physical Review Letters*, 112, 051303
 Bennett C. L. et al., 2013, *ApJS*, 208, 20
 Bize S. et al., 2003, *Phys. Rev. Lett.*, 90, 150802
 Bonifacio P. et al., 2014, *Astronomische Nachrichten*, 335, 83
 Challinor A., Peiris H., 2009, in *American Institute of Physics Conference Series*, Vol. 1132, American Institute of Physics Conference Series, Novello M., Perez S., eds., pp. 86–140
 Chluba J., Ali-Haïmoud Y., 2016, *MNRAS*, 456, 3494
 Chluba J., Fung J., Switzer E. R., 2012, *MNRAS*, 423, 3227
 Chluba J., Sunyaev R. A., 2006a, *A&A*, 458, L29
 Chluba J., Sunyaev R. A., 2006b, *A&A*, 446, 39
 Chluba J., Sunyaev R. A., 2007, *A&A*, 475, 109
 Chluba J., Sunyaev R. A., 2008, *A&A*, 480, 629
 Chluba J., Sunyaev R. A., 2009a, *A&A*, 503, 345
 Chluba J., Sunyaev R. A., 2009b, *A&A*, 496, 619
 Chluba J., Thomas R. M., 2011, *MNRAS*, 412, 748
 Chluba J., Vasil G. M., Dursi L. J., 2010, *MNRAS*, 407, 599
 Coc A., Uzan J.-P., Vangioni E., 2013, ArXiv:1307.6955
 Di Valentino E. et al., 2016, ArXiv:1612.00021
 Drake G. W. F., 2006, *Springer Handbook of Atomic, Molecular, and Optical Physics*. Springer
 Fendt W. A., Chluba J., Rubiño-Martín J. A., Wandelt B. D., 2009, *ApJS*, 181, 627
 Galli S., Martins C. J. A. P., Melchiorri A., Menegoni E., 2011, *Astrophysics and Space Science Proceedings*, 22, 59
 Grachev S. I., Dubrovich V. K., 2008, *Astronomy Letters*, 34, 439
 Gratton S., Lewis A., Efstathiou G., 2008, *Phys.Rev.D*, 77, 083507
 Hirata C. M., 2008, *Phys.Rev.D*, 78, 023001
 Hirata C. M., Forbes J., 2009, *Phys.Rev.D*, 80, 023001

- Hu W., Sugiyama N., 1996, *ApJ*, 471, 542
- Kaplinghat M., Scherrer R. J., Turner M. S., 1999, *Phys.Rev.D*, 60, 023516
- Karzas W. J., Latter R., 1961, *ApJS*, 6, 167
- Kholupenko E. E., Ivanchik A. V., Varshalovich D. A., 2007, *MNRAS*, 378, L39
- Kotuš S. M., Murphy M. T., Carswell R. F., 2017, *MNRAS*, 464, 3679
- Lewis A., Bridle S., 2002, *Phys. Rev.*, D66, 103511
- Lewis A., Challinor A., Lasenby A., 2000, *ApJ*, 538, 473
- Lorén-Aguilar P., García-Berro E., Isern J., Kubyshev Y. A., 2003, *Classical and Quantum Gravity*, 20, 3885
- Martins C. J. A. P., Melchiorri A., Rocha G., Trotta R., Avelino P. P., Viana P. T. P., 2004, *Physics Letters B*, 585, 29
- Martins C. J. A. P., Menegoni E., Galli S., Mangano G., Melchiorri A., 2010, *Phys.Rev.D*, 82, 023532
- Menegoni E., Archidiacono M., Calabrese E., Galli S., Martins C. J. A. P., Melchiorri A., 2012, *Phys.Rev.D*, 85, 107301
- Mukhanov V., 2004, *International Journal of Theoretical Physics*, 43, 623
- Peebles P. J. E., 1968, *ApJ*, 153, 1
- Peebles P. J. E., Yu J. T., 1970, *ApJ*, 162, 815
- Planck Collaboration et al., 2015a, *ArXiv:1502.01589*
- Planck Collaboration et al., 2015b, *A&A*, 580, A22
- Rich J., 2015, *A&A*, 584, A69
- Rocha G., Trotta R., Martins C. J. A. P., Melchiorri A., Avelino P. P., Bean R., Viana P. T. P., 2004, *MNRAS*, 352, 20
- Rosenband T. et al., 2008, *Science*, 319, 1808
- Rubiño-Martín J. A., Chluba J., Fendt W. A., Wandelt B. D., 2010a, *MNRAS*, 403, 439
- Rubiño-Martín J. A., Chluba J., Fendt W. A., Wandelt B. D., 2010b, *MNRAS*, 403, 439
- Rubiño-Martín J. A., Chluba J., Sunyaev R. A., 2006, *MNRAS*, 371, 1939
- Rubiño-Martín J. A., Chluba J., Sunyaev R. A., 2008, *A&A*, 485, 377
- Scóccola C. G., Landau S. J., Vucetich H., 2009, *Memorie della Societ Astronomica Italiana*, 80, 814
- Seager S., Sasselov D. D., Scott D., 1999, *ApJL*, 523, L1
- Seager S., Sasselov D. D., Scott D., 2000, *ApJS*, 128, 407
- Shaw J. R., Chluba J., 2011, *MNRAS*, 415, 1343
- Sobolev V. V., 1960, *Moving envelopes of stars*. Cambridge: Harvard University Press, 1960
- Sunyaev R. A., Chluba J., 2009, *Astronomische Nachrichten*, 330, 657
- Sunyaev R. A., Zeldovich Y. B., 1970, *ApSS*, 7, 3
- Switzer E. R., Hirata C. M., 2008, *Phys.Rev.D*, 77, 083006
- Uzan J.-P., 2003, *Reviews of Modern Physics*, 75, 403
- Uzan J.-P., 2011, *Living Reviews in Relativity*, 14, 2
- Zeldovich Y. B., Kurt V. G., Syunyaev R. A., 1968, *Zhurnal Eksperimentalnoi i Teoreticheskoi Fiziki*, 55, 278

This paper has been typeset from a $\text{\TeX}/\text{\LaTeX}$ file prepared by the author.